JJEE
Volume 10 | Number 1 | March 2024 | Pages 103-121

Jordan Journal of Electrical Engineering

ISSN (print): 2409-9600, ISSN (online): 2409-9619

Homepage: jjee.ttu.edu.jo

Experimental and Simulated Investigation of a Single-Phase Transformerless H5 Inverter Topology

Hakki Mollahasanoglu[1*], Emre Ozkop[2]

[1] Department of Electrical and Electronics Engineering, Recep Tayyip Erdogan University, Rize, Turkey
E-mail: hakki.mollahasanoglu@erdogan.edu.tr
[2] Department of Electrical and Electronics Engineering, Karadeniz Technical University, Trabzon, Turkey

Received: May 08, 2023 *Revised: July 17, 2023* *Accepted: July 22, 2023*

***Abstract*—** This paper aims to simulate and experimentally apply a single-phase transformerless H5 inverter topology. The H5 inverter topology is simulated in MATLAB/Simulink environment as both off-grid and grid-connected. The simulation results of the grid-connected system are evaluated in terms of output voltage/current, total harmonic distortion (THD), and injected active and reactive powers into the grid. The off-grid system is evaluated regarding load current, inverter output voltage, efficiency, and THD. Despite the variable output load, the results offer good THD values that comply with the IEEE 1547 standard. Additionally, experimental studies are conducted on the single-phase off-grid transformerless H5 inverter. A digital processing unit is utilized to control and display the output voltage of the H5 inverter system in real-time mode. PI and Fuzzy PI controllers are used for output voltage control. The obtained results reveals that the investigated topology outperforms its counterparts.

***Keywords*—**Grid-connected inverter; H5 inverter; Transformerless inverter; Total harmonic distortion; Off-grid inverter; TMS320DOCKF28335 kit.

Nomenclature

ADC	Analog/digital converter	PLL	Phase locked loop
DC	Direct current	PWM	Pulse width modulation
DSP	Digital signal processor	SPWM	Sinusoidal pulse width modulation
HBZVR	H-bridge zero-voltage rectifier	THD	Total harmonic distortion
FB-DCBP	Full-bridge inverter with DC bypass	TI	Texas instrument
HB-NPC	Half-bridge neutral point clamped	V_{cm}	Common mode output voltage
HERIC	Highly efficient and reliable inverter concept	f_{sw}	Switching frequency
IAE	Integral of the absolute error	V_f	Forward voltage
ISE	Integral of the square error	R_{ff} - L_{ff}	Feedforward and remove disturbance
ITAE	Integral of time multiplied by the absolute error	R_L	Variable load
NPC	Neutral point clamped	V_L	Output voltage
PI	Proportional integral	η	Efficiency

* Corresponding author
Article's DOI: 10.5455/jjee.204-1683544600

1. INTRODUCTION

The interest in renewable energy sources has increased rapidly over the past few years, and solar energy has emerged as one of the most favored alternatives [1, 2]. The rapid advancements in semiconductor technology have contributed significantly to the popularity of solar energy. In the context of solar energy, inverters play a crucial role in transferring the electric energy generated from solar systems to the grid or load, ensuring that it follows the electrical system's characteristics. Inverters used in photovoltaic systems can be classified into two types- those with transformers and those that are transformerless.

The former type of inverter typically consists of a transformer that steps up the voltage generated by the solar panels. On the other hand, transformerless inverters are smaller in size and do not use transformers. They rely on capacitors and other electronic components to convert voltage. Transformerless inverters are preferred over conventional inverters because of their cost-effectiveness, smaller size, lighter weight, and simpler structure [3, 4].

However, transformerless PV inverters have a leakage current problem since there is no transformer. They must adhere to standards such as IEEE 1547.1, VDE0126-1-1, EN 50106, IEC61727, and AS/NZS 5033 [5, 6]. These standards consider total harmonic distortion (THD) and current harmonic levels, injected DC and leakage current, voltage and frequency range for efficient operation, and power factor. Therefore, transformerless inverter topologies have been developed in the literature, depending on the number of switches, modulation types used, THD, or leakage current.

Several inverter topologies exist, including H5, H6, H7, H8, HERIC, HB-ZVR, HB-DCBP, and NPC [5–11]. These topologies are derived from H-bridge or full-bridge inverters and are related to each other. Therefore, they can be evaluated and compared from various perspectives. For example, the H5, HERIC, H6, H7, and H8 inverter topologies were developed based on a full-bridge inverter to maintain a constant common mode voltage [10–13]. Some studies have attempted to reduce the common mode voltage effect by using active neutral point clamp-based PN-NPC [14], HB-ZVR [15], HB-ZVR-D [16], and HB-ZVSCR topologies.

The H5 inverter topology is more practical than other topologies due to its simpler structure and fewer switches. Studies have shown that the leakage current amount of the H5 inverter topology is low, and its efficiency is high [17]. Furthermore, increasing the switching frequency has been found to reduce the total harmonic distortion in the H5 inverter topology [18]. The H5 inverter topology, widely used in single-phase systems, can be converted into a three-phase structure by cascading, which effectively reduces the leakage current amount [19]. It is important to note that THD and leakage current vary depending on the applied modulation technique, with bipolar modulation performing better than hybrid modulation [20, 21].

The objective of this study is to investigate and analyze the performance of single-phase transformerless H5 inverter systems in various scenarios, including off-grid and grid-connected, to supply energy to the grid or any load. To achieve this, a simulation of the transformerless H5 inverter topology independent from the grid was conducted using the MATLAB/Simulink platform. Additionally, experimental studies were performed on off-grid structures to gather data for comparison with the simulation results. The motivation behind this study is to explore the potential use of single-phase transformerless H5 inverter systems in various applications. The significance of this study is that it provides insights into the performance of single-phase transformerless H5 inverter systems, which can be used to

improve their use in different applications. The simulation and experimental studies conducted in this research provide a better understanding of the behavior of these systems and can help to optimize their design and performance.

2. TRANSFORMERLESS H5 INVERTER TOPOLOGY AND OPERATING MODES ANALYSIS

The H5 topology is a common option for transformerless inverters, designed specifically to prevent leakage current in single-phase PV systems. It involves adding a fifth switching element to the DC side of the H-bridge inverter. The fifth switch operates at high frequencies, isolating the PV module from the circuit during zero voltage transition [22]. This prevents reactive power flow between the system input capacity and the filter inductance at the inverter output. Fig. 1 shows the general circuit diagram of the H5 topology. In the H5 topology, two switches are operated at the system frequency, while the others are operated at a higher frequency. The operating states of the H5 inverter are shown in Fig. 2.

Fig. 3 shows the Sinusoidal Pulse Width Modulation (SPWM) signals for the switches. SPWM is a widely used modulation technique that provides a sinusoidal output, low harmonic distortion, high energy efficiency and has a wide application area.

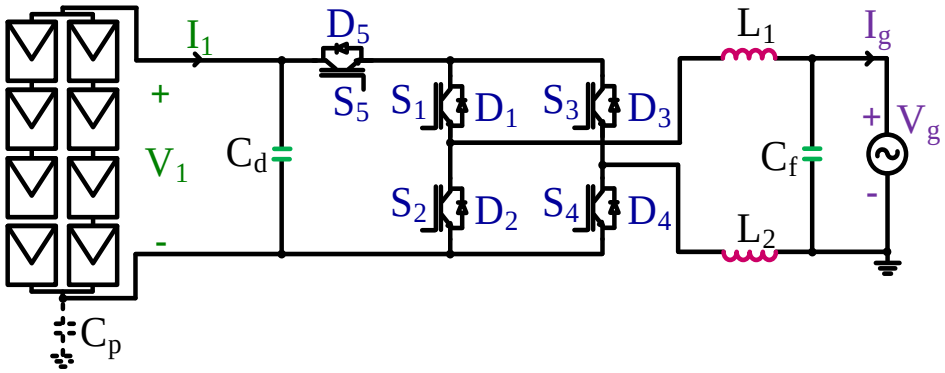

Fig. 1. General circuit diagram of the H5 topology.

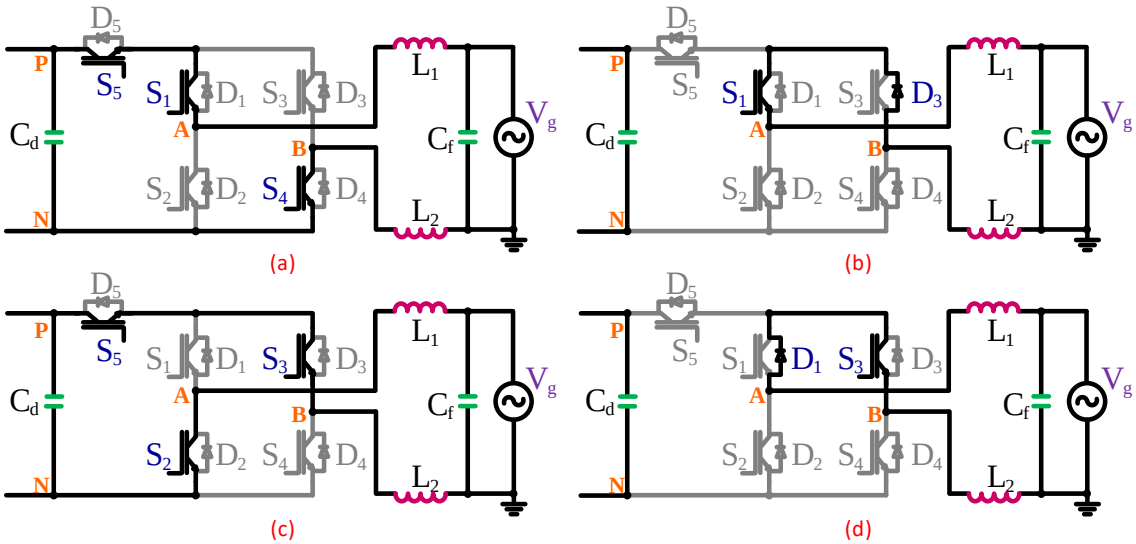

Fig. 2. Operating modes of the H5 inverter topology.

SPWM generates a sinusoidal voltage at the inverter output, resulting in low harmonic distortion in the output current, thus achieving high energy efficiency in applications.

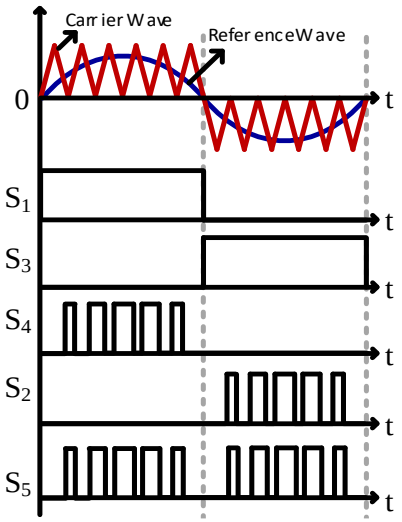

Fig. 3. H5 inverter switching signals.

This modulation technique compares the reference sinusoidal signal with the triangular carrier signals, and the resulting pulse width occurs in sinusoidal form. The H5 inverter topology has five switching elements. Switches S_1 and S_3 are triggered at the grid frequency, with S_1 continuously operating and S_3 in cutoff mode. Switches S_2 and S_4 are switched at high frequency by variable pulse width, which is proportional to the amplitude of the sine wave. By comparing the triangular carrier signals with a reference sine signal, S_2 and S_4 are operated efficiently using Pulse Width Modulation (PWM) techniques.

Fig. 2(a) shows the active operating state. The high frequency switch is denoted by S_5 and the system frequency switch by S_1. The current flows through switches S_5-S_1 and S_4. In the active operating state, $V_{AB} = +V_{PN}$. The common mode output voltage is calculated using Eq. (1).

$$V_{cm} = \frac{1}{2}(V_{AN} + V_{BN}) = \frac{1}{2}(V_{PN} + 0) = \frac{V_{PN}}{2} \quad (1)$$

In Fig. 2(b), the direction of current flow is from switch S_1 to diode D_3 as a released loop. In this operating state, $V_{AB} = 0$, and the common mode output voltage value is calculated as in Eq. (2).

$$V_{cm} = \frac{1}{2}(V_{AN} + V_{BN}) = \frac{1}{2}\left(\frac{V_{PN}}{2} + \frac{V_{PN}}{2}\right) = \frac{V_{PN}}{2} \quad (2)$$

In the active operating state shown in Fig. 2(c), S_5 is switched at high frequency while S_2 is switched at the system frequency. Current flows through the switches S_5-S_3 and S_2. In this state, $V_{AB} = -V_{PN}$, and the common-mode output voltage value is calculated using Eq. (3).

$$V_{cm} = \frac{1}{2}(V_{AN} + V_{BN}) = \frac{1}{2}(0 + V_{PN}) = \frac{V_{PN}}{2} \quad (3)$$

In Fig. 2(d), the current flows through switch S_3 and diode D_1 as part of the released loop. In this operating state, V_{AB} is 0, and the common mode output voltage value is calculated using Eq. (4).

$$V_{cm} = \frac{1}{2}(V_{AN} + V_{BN}) = \frac{1}{2}\left(\frac{V_{PN}}{2} + \frac{V_{PN}}{2}\right) = \frac{V_{PN}}{2} \quad (4)$$

The variable V_{cm} represents the common mode output voltage in the equations. It can be observed that V_{cm} remains constant at a value of $V_{PN}/2$ for the switching situations mentioned above. Therefore, the unipolar modulation technique for the H5 inverter can maintain a constant output voltage.

3. SIMULATION RESULTS

The single-phase transformerless H5 inverter simulation study has been conducted using MATLAB/Simulink for both off-grid and grid-connected scenarios. This study aimed to evaluate the performance of the H5 inverter under different conditions and assess its suitability for both off-grid and grid-connected applications.

3.1. The Off-Grid Transformerless H5 Inverter

The off-grid transformerless H5 inverter system was analyzed using a simulation model whose block diagram is shown in Fig. 4. The system's performance is evaluated regarding the inverter's output voltage, load current, voltage, and THD.

The simulation model of the H5 inverter system shown in Fig. 4 can be used to control the inverter output voltage using simulation software.

The control can be achieved using Proportional Integral (PI) controllers or Fuzzy Proportional Integral controllers (Fuzzy PI). The parameter values for the simulation study are provided in Table 1.

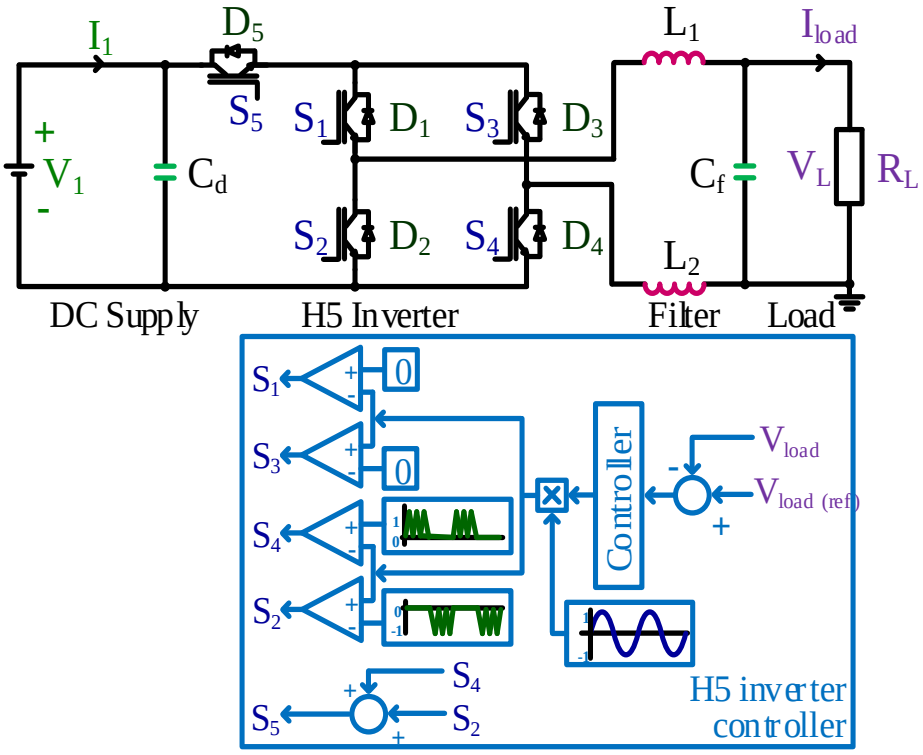

Fig. 4. Block diagram for the simulation model of the H5 inverter system.

Table 1. Parameters used in the simulation.

Load	Supply	LCL Filter	Controller	H5 Inverter
50 Hz	$V_1 = 50$ V	$L_1 = 40$ mH	$K_p = 0.003$	$f_{sw} = 10$ kHz
0-500 Ω	$C_d = 10$ mF	$L_2 = 40$ mH	$K_i = 0.51$	-
-	-	$C_f = 650$ nF	-	-

The simulation results, shown in Fig. 5, display the inverter output voltage, load current, and load voltage for an output voltage ($V_{load} = 220$ V (rms)) and load ($R_{load} = 100$ Ω).

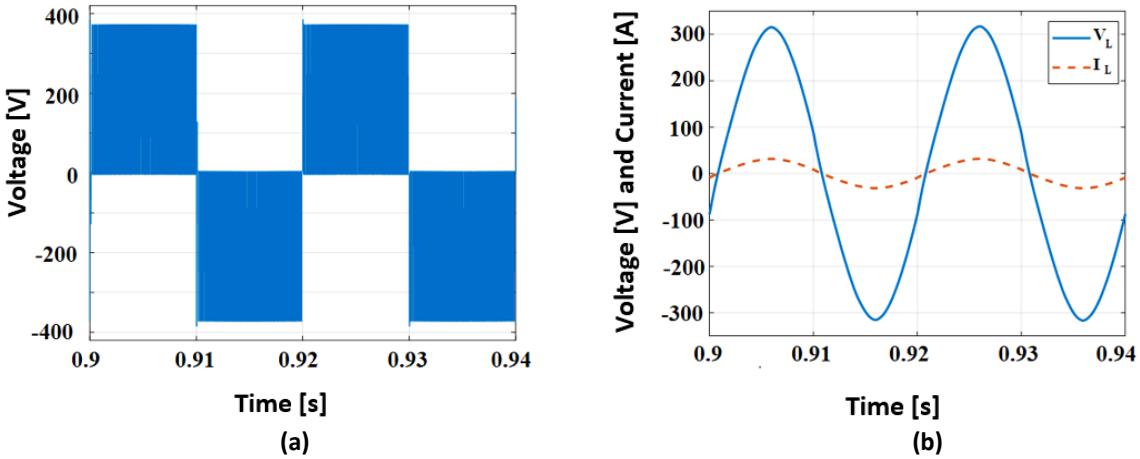

Fig. 5. a) Output voltage; b) Load voltage and load current (x10) of the H5 inverter

The total harmonic distortion (THD) analysis of the load voltage was conducted using MATLAB/Simulink environment. The results are presented in Fig. 6 and Table 2. Based on Table 2, the total and graded harmonic distortion values of the voltage are lower than the standards set in [23].

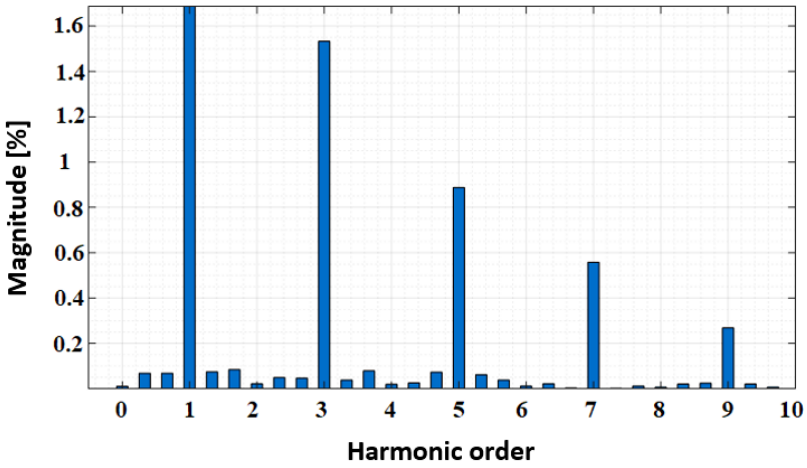

Fig. 6. FFT analysis of the load voltage.

Table 2. Harmonic distortion distribution on load voltage.

	THD [%]	3rd [%]	5th [%]	7th [%]	9th [%]
Simulation results	1.91	1.53	0.89	0.56	0.27
IEEE 1547	≤5.00	≤4.00	≤4.00	≤4.00	≤4.00

However, it should be noted that the use and reference of this standard should primarily be for the grid-connected version of the inverter. The main purpose of comparing the standard (IEEE 1547) in Table 2 is to show the status of the simulated inverter system according to standard values.

While the system's input and output voltage values remain constant, the inverter's input and output current and voltage values are observed for different loads. The input and output power values are then calculated, and the inverter efficiency is determined. An experimental study was conducted for an output voltage of $V_L = 35$ V and a variable load (R_L). The observed current, voltage, calculated power, and efficiency are summarized in Table 3.

Table 3. Results of H5 inverter efficiency test-I.

Input			Output			Efficiency	Load
V_1 [V]	I_1 [A]	P_1 [W]	V_L [V]	I_L [A]	P_L [W]	η [%]	R_L [Ω]
50	0.3126	15.567	34.5	0.417	14.442	92.775	50
50	0.2541	12.666	34.8	0.333	11.622	91.756	68
50	0.1836	9.159	34.8	0.236	8.254	90.117	100
50	0.1275	6.364	35.4	0.150	5.326	83.690	150
50	0.0901	4.503	35.8	0.096	3.460	76.844	220
50	0.0634	3.168	36.0	0.062	2.255	71.180	470

The efficiency of the system decreases as the load value at the system output increases. An experimental study has been conducted for $V_L = 20$ V and variable load (R_L), as shown in Table 4. The study observed the inverter input and output current for different load values, the calculated input and output powers, the inverter efficiency, and the load value. When Table 3 and 4 are examined, it can be observed that the input voltage (V_1) is constant throughout the entire measurement and the output voltage value (V_L), although not much, decreases as the current value drawn by the load increases (which occurs as the resistive value of the load (R_L) decreases).

Due to the converter input voltage being higher than the output voltage, it was observed that the input current (I_1) is closer the output current (I_L), especially at high load values, and that the output current value reaches the input current value when the load value is reduced and then passes it. When the input and output current and voltage values are compared, it was observed that the converter efficiency is low at low power levels and the converter performance is high at high power levels.

Table 4. Results of H5 inverter efficiency test-II.

Input			Output			Efficiency	Load
V_1 [V]	I_1 [A]	P_1 [W]	V_L [V]	I_L [A]	P_L [W]	η [%]	R_L [Ω]
50	0.2132	10.617	19.4	0.425	8.288	78.067	50
50	0.1546	7.706	19.4	0.302	5.864	76.096	68
50	0.1077	5.373	19.6	0.199	3.924	73.032	100
50	0.0733	3.662	19.7	0.130	2.567	70.099	150
50	0.0515	2.572	19.7	0.083	1.651	64.199	220
50	0.0291	1.456	19.9	0.042	0.845	58.021	470

Fig. 7 illustrates the variation in efficiency-output power for different output voltage (V_L) levels. Upon examining Fig. 7, it can be observed that the system efficiency decreases as the load voltage value decreases. Specifically, as the output voltage value decreases from 35 volts to 20 volts, the efficiency value also decreases. One of the main reasons is that power is a function of current and voltage. In a system with constant voltage, the system's output power depends directly on the variation of current. At the same power level, the current value in low voltage ($V_L = 20$ V) is higher than in high voltage ($V_L = 35$ V). Therefore, high current flow causes high switching power loss and results in lower efficiency, as shown in Fig. 7.

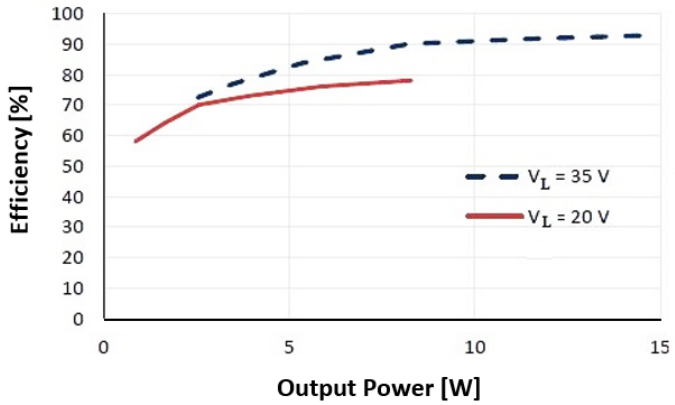

Fig. 7. Efficiency versus output power for different output voltage (V_L) levels.

The system's output voltage control is achieved using Proportional Integral (PI) and Fuzzy PI controllers in the simulation study. The waveforms for output voltage and output current, as well as ISE, IAE, and ITAE performance criteria, are analyzed. These performance criteria consider the error and relate it to time. The Integral of the Square Error (ISE) is the most preferred performance criterion as it integrates the square of the error at the control system output over time. The Integral of the Absolute Error (IAE) treats all deviations from the steady-state value equally.

On the other hand, the Integral of Time multiplied by the Absolute Error (ITAE) gives more weight to deviations from the steady-state value, with earlier deviations being less weighted than later ones. This is achieved by multiplying the error by time. These criteria are used during the design and adjustment of control systems to evaluate how close the output of the control system is to the target value and to assess stability by minimizing their values.

This study compares PI controller and fuzzy logic PI controller to control a system with H5 inverter topology. These control methods have some key differences. The PI control method requires precise parameter settings and is based on mathematical modelling. This method works well for linear systems, and parameter adjustments can be made to achieve optimum control performance.

On the other hand, the fuzzy PI control method uses fuzzy logic-based rules, which provide a more flexible parameter-setting process. This method offers a more adaptable approach to dealing with system uncertainties.

Fuzzy logic PI control can be effective in more demanding applications, such as non-linear and complex systems, due to its ability to adapt to uncertain situations and handle uncertainties in the system. Initially, the PI controller block was used, and the simulation result is presented in Fig. 8.

The simulation study was conducted using the Fuzzy PI controller. The controller's input parameters are determined by the error ($e(k)$) and change in error ($de(k)$), and the output is determined accordingly.

The Fuzzy PI controller's output (du) determines the switch duty cycle, allowing control of the inverter. Eqs. (5) and (6) show the mathematical expressions for the error change and error.

$$de(k) = e(k) - e(k-1) \quad (5)$$

$$e(k) = V_{ref} - V_0(k) \quad (6)$$

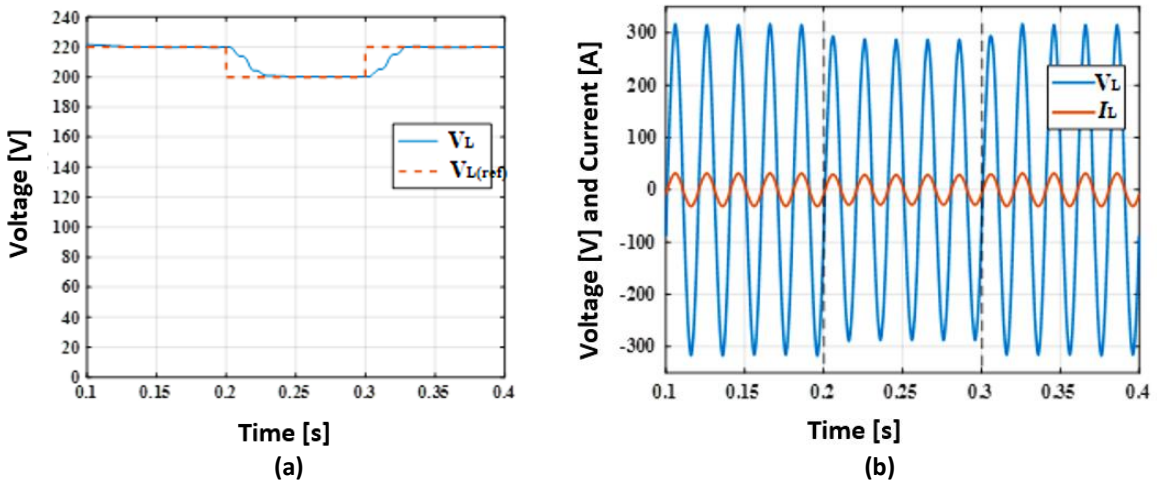

Fig. 8. a) Output voltage and reference voltage; b) load voltage and load current (x10) of the PI controller.

The Mamdani (max-min approximation) method was used for inference, and the area's central method was used for defuzzification. The simulation results are shown in Fig. 9.

Table 5 presents the performance results of the obtained PI and Fuzzy PI controllers for voltage control of the system.

Based on Table 5, the Fuzzy PI controller provides better results than the PI controller regarding ISE, IAE, and ITAE criteria.

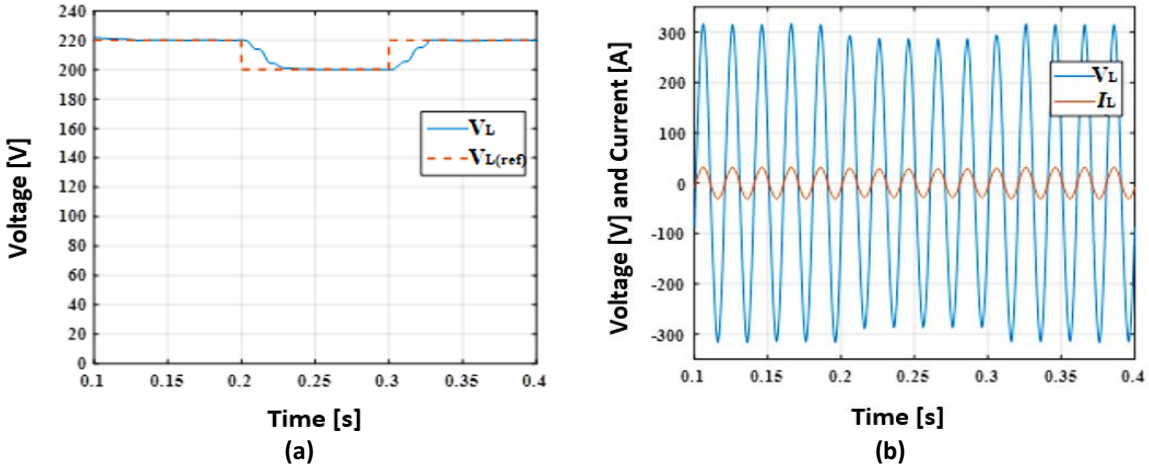

Fig. 9. a) Output voltage and reference voltage; b) load voltage and load current (x10) of the Fuzzy PI controller.

Table 5. Comparison of control methods.

Controller	ISE	IAE	ITAE	THD [%]
PI	12.58	0.8580	0.2155	1.90
Fuzzy PI	12.24	0.8038	0.1932	1.90

3.2. The Grid Connected Transformerless H5 Inverter

The general block diagram of the single-phase grid connected H5 inverter system without a transformer is shown in Fig. 10.

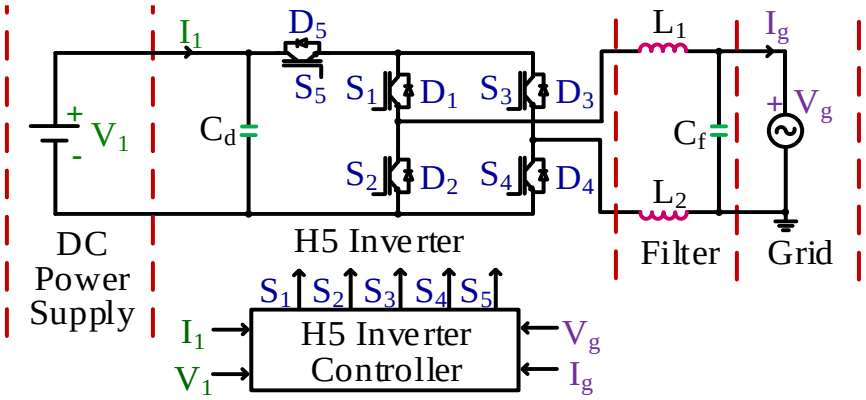

Fig. 10. General block diagram of the single-phase grid-connected transformerless H5 inverter system.

The H5 inverter converts DC to AC while minimizing disturbances with the LCL filter. The H5 inverter control system utilizes cascade control based on the AC current drawn from the grid and DC input voltage. Fig. 11 shows the general block diagram of the grid connected H5 inverter system controller. By using the DC input voltage, the current to the grid is determined as a reference and the voltage waveform is obtained.

Here, R_{ff} and L_{ff} represent the feedforward and disturbance removal parameters, respectively. Grid amplitude and frequency are crucial parameters in grid-connected inverter systems.

The grid voltage information is essential for current synchronization with the grid. This voltage information is obtained using the phase-locked loop (PLL) technique.

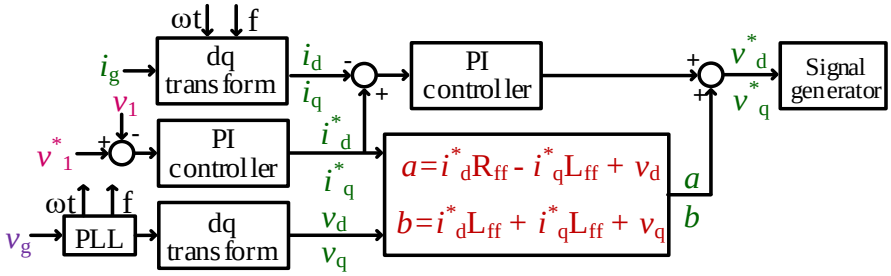

Fig. 11. General block diagram of the grid-connected H5 inverter system [24].

The grid voltage and transferred current information are then converted to the d-q axis. The required reference voltage values for pulse width modulation (PWM) are obtained using a PI controller, and inverter control is provided to obtain the reference signals required for inverter operation under IEEE 1547 standards.

The system's performance is evaluated based on the inverter output voltage, grid current and voltage, active and reactive power, and total harmonic distortion (THD). The parameter values of the elements used in the simulation study are given in Table 6.

Table 6. Model parameters utilized in the simulation of the grid connected H5 inverter system.

Grid and DC Supply		H5 inverter		Controller		Filter	
Frequency	50 Hz	f_{sw}	10 kHz	R_{ff}	2 mΩ	L_1	2.18 mH
Voltage	240 V	V_f (IGBT)	2.5 V	L_{ff}	0.2 H	L_2	2.18 mH
V_1	400 V	V_f (Diode)	1.6 V	K_p	12	C_f	2 nF
C_d	10 mF	-	-	K_i	200	-	-

Table 6 shows the values of f_{sw} and V_f, which represent the switching frequency and forward voltages of the semiconductor elements, respectively. The simulation study yields result for the inverter output voltage, the transferred current to the grid, and grid voltage waveforms, as shown in Fig. 12.

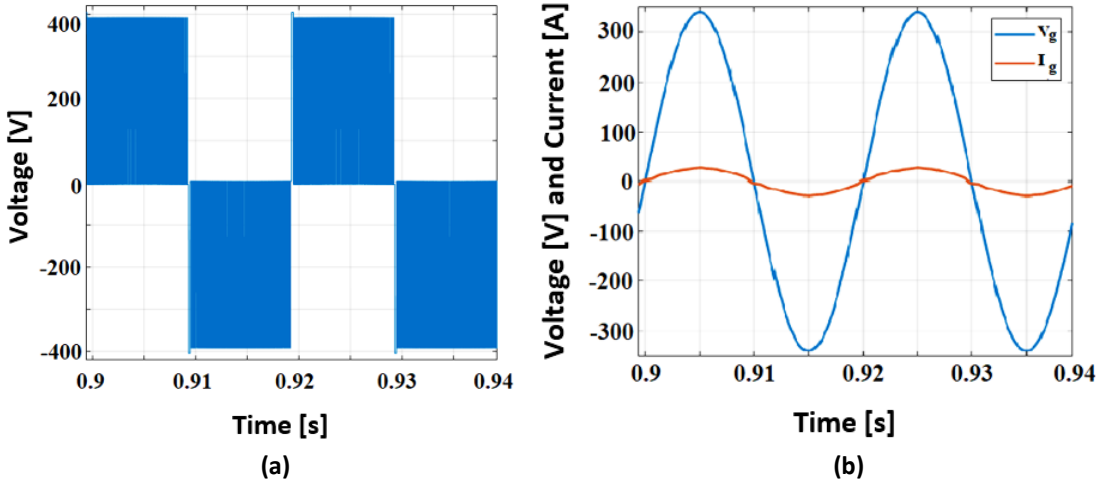

Fig. 12. a) Inverter output voltage; b) grid voltage and current (x10).

Harmonics play a significant role in power electronics circuits. Harmonic distortion in current and voltage in power systems can have negative effects. Fourier analysis can be used to perform harmonic analysis easily. This study examines the harmonic analysis of the single-phase grid-connected transformerless H5 inverter system in terms of total harmonic distortion (THD). Fig. 13 shows the harmonic on grid current, and Table 5 provides the corresponding numerical values.

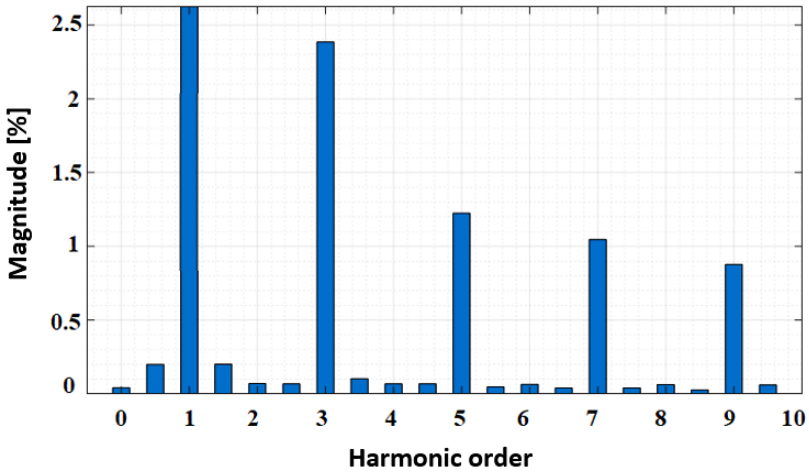

Fig. 13. FFT analysis of the current transferred to the grid.

Based on Table 7, the current total and graded harmonic distortion values are lower than the specified values in IEEE 1547. Fig. 14 shows the graphs of active and reactive power injected into the grid over time.

Table 7. Harmonic distortion distribution of the current transferred to the grid.

	THD [%]	3rd [%]	5th [%]	7th [%]	9th [%]
Simulation results	3.82	2.39	1.22	1.05	0.88
IEEE 1547	≤5.00	≤4.00	≤4.00	≤4.00	≤4.00

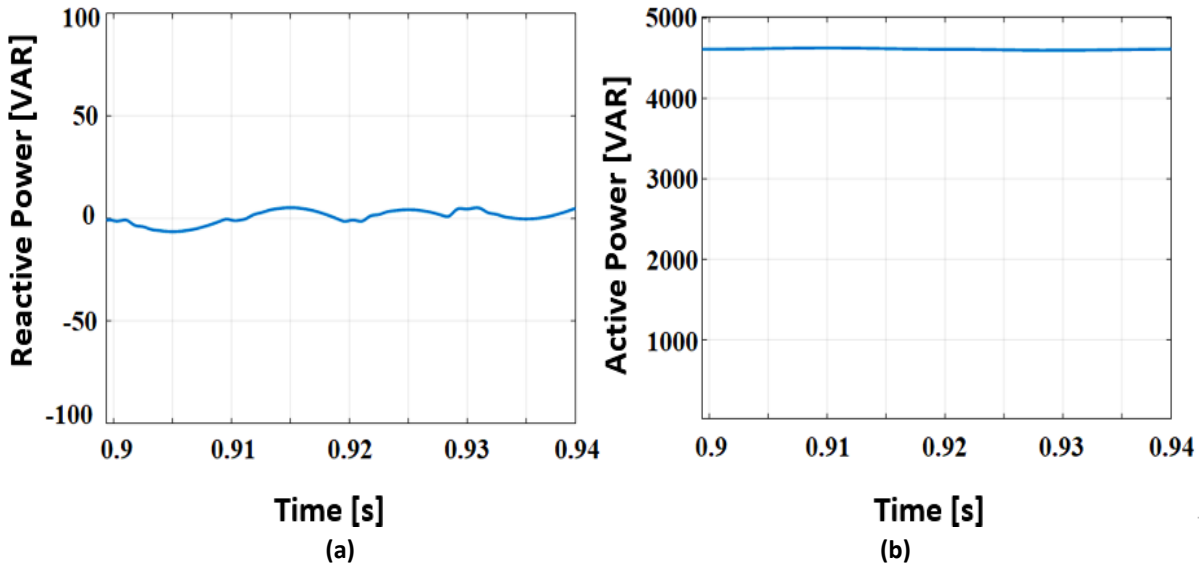

Fig. 14. Power transferred to the grid: a) the reactive power; b) the active power.

The active power being injected into the grid changes according to the current and voltage values at the output of the inverter. The reactive power is maintained at a minimum level.

4. EXPERIMENTAL INSTALLATION AND RESULTS

The designed single-phase off-grid transformerless H5 inverter system is comprised of a DC power supply, H5 inverter and driver circuit, LCL filter, current-voltage sensor circuits, analogue circuit, and TMS320F28335 digital signal processor (DSP) components. The experimental setup block diagram is shown in Fig. 15.

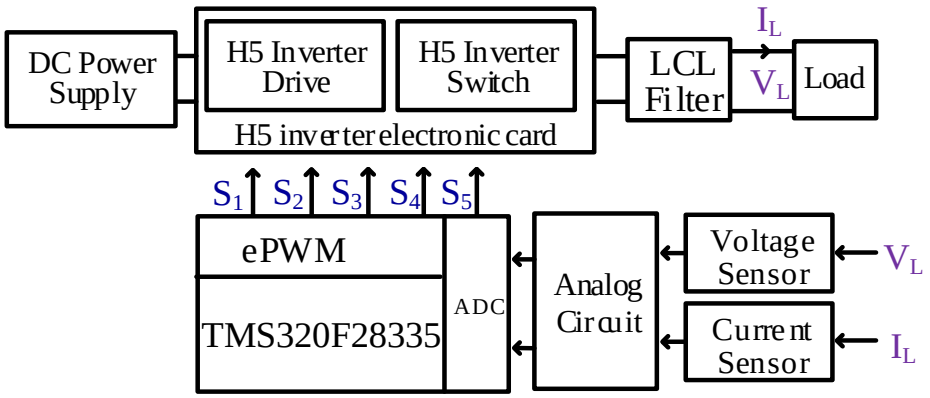

Fig. 15. Block diagram of the experimental setup.

The block diagram depicted in Fig. 15 has been implemented as an experimental application, as shown in Fig. 16.

The load current and voltage values at the inverter output are determined by current and voltage sensor circuits. Using an analogue circuit, they are then reconverted for the digital signal processor (DSP). The ADC block of the DSP is suitable for data inputs between 0-3.3 volts. Therefore, the voltage value is reduced by 1/50 and then transferred to the analog/digital converter (ADC) block.

Fig. 16. The experimental setup (a: oscilloscope, b: TMS320DOCKF28335 kit c: isolation circuit d: H5 inverter and drive, e: Filter, f: Analog circuit, g: voltage sensor circuits, h: voltage analyzer, i: DC Supplies.)

Each switch's pulse width modulation (PWM) signals are generated using a control algorithm created in the MATLAB/Simulink interface, depending on the voltage values from the ADC block. Switches S_1 and S_3 are triggered at grid frequency while S_2, S_4 and S_5 are switched at high frequency. The H5 inverter switching signals are shown in Fig. 17.

Each switch is controlled by the signals transmitted from the digital input-output of the DSP to the switch driver circuit.

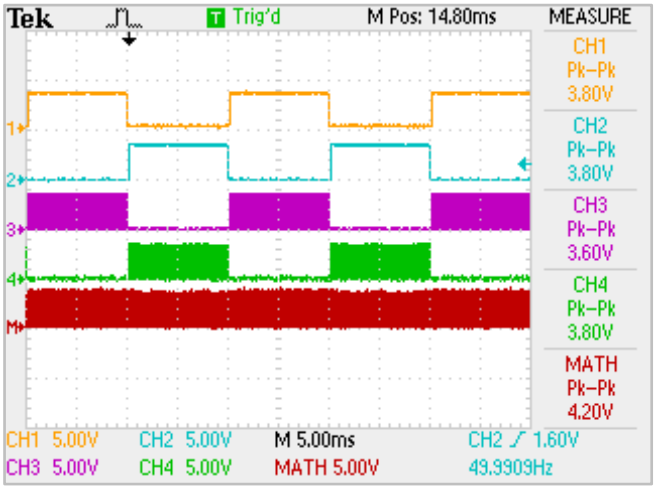

Fig. 17. H5 inverter switching signals.

S_1, S_2 and S_3, S_4 switches are connected in series on each leg of the H5 inverter, and the switches' triggering times can intersect. A dead time has been added to the MATLAB/Simulink environment switching time to prevent short circuits on the serial switches. The switches can be damaged without the dead time, and the system may operate noisily.

This study utilized the TMS320DOCKF28335 kit developed by Texas Instruments (TI). This card is commonly used in control applications, such as robotics, industrial automation,

and power supplies. It is the main component of the TMS320DOCKF28335 kit and features easy plug-in capabilities [25]. Table 8 displays the features of the kit.

The microcontroller was selected for its high RAM capacity and operating frequency. Developed by TI, the C2000 plug-in enables the programming of the company's digital signal processors in the MATLAB/Simulink environment. This allows ready-made blocks such as PWM, ADC, and QEP, included in the TMS320DOCKF28335 kit, to be converted into digital code and transferred to the digital signal processor simultaneously. The USB input and Simulink interface on the computer support external mode, making this possible. These are the main reasons why the kit was selected for this study.

Table 8. Technical specifications of the TMS320DOCKF28335 kit [25].

Specification	Value
CPU	32 Bit
Speed	150 MHz
RAM	68 KB
Memory	512 KB
ADC	16 (12 bit 25 MHz)
GPIO	88
PWM	18
External RAM	No

The TMS320DOCKF28335 kit supplies the required switching signals for the H5 inverter driver card and controls the duty cycle. Fig. 18 shows the output voltage waveforms of the system at 0.5 and 0.85 duty cycle (for a 50 V inverter input voltage).

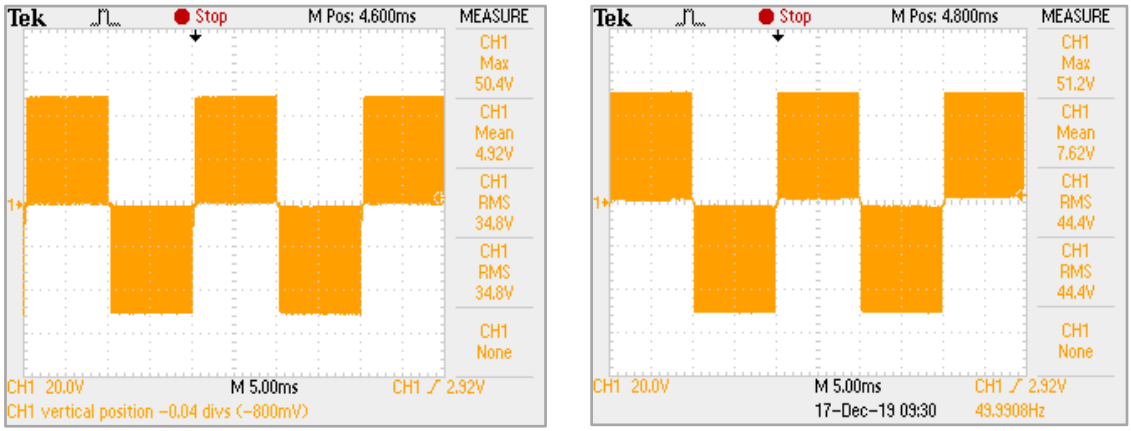

Fig. 18. Output voltage of the H5 inverter at duty cycles of: a) 0.5; b) 0.85.

Based on Fig. 18, the inverter output voltage increases when the duty cycle of the H5 inverter switch increases. Therefore, the output voltage can be adjusted by changing the duty cycle of the inverter.

The analog circuit is designed to read the AC signal from the ADC pin of the control card. To make the signal suitable for the ADC block, the negative alternations of the AC signal have been removed on the axis. The ADC block has a measurement range between 0 and 3.3 Volts. Two different studies were conducted to study the system experimentally. The first

study focused on examining the H5 inverter efficiency. The second study involved comparing different control methods.

While the system's input and output voltage values remain constant, the inverter's input and output current and voltage values are measured for different loads. The input and output power values are then calculated, and the inverter efficiency is determined. An experimental study was conducted for an output voltage value of $V_L = 35$ V and a variable load (R_L). The observed current, voltage, calculated power, and efficiency values are summarized in Table 9.

Table 9. Results of H5 inverter efficiency test-I.

Input			Output			Efficiency	Load
V_1 [V]	I_1 [A]	P_1 [W]	V_L [V]	I_L [A]	P_L [W]	η [%]	R_L [Ω]
50	0.591	29.470	34.188	0.666	22.800	77.366	50
50	0.460	22.935	34.547	0.504	17.445	76.065	68
50	0.315	15.744	34.645	0.339	11.760	74.696	100
50	0.220	11.037	34.961	0.229	8.034	72.789	150
50	0.154	07.725	34.990	0.155	5.454	70.607	220
50	0.073	03.696	35.279	0.073	2.587	69.995	470

As the load value at the system output increases, the system efficiency decreases. Table 10 shows the results of an experimental study conducted for $V_L = 20$ V and variable load (R_L).

The study observed the inverter input and output current for different load values, calculated input and output powers, inverter efficiency, and load value.

When Table 10 are examined, it can be observed that the input voltage (V_1) is constant throughout the entire measurement and the output voltage value (V_L), although not much, decreases as the current value drawn by the load increases (which occurs as the resistive value of the load (R_L) decreases).

Table 10. Results of H5 inverter efficiency test-II.

Input			Output			Efficiency	Load
V_1 [V]	I_1 [A]	P_1 [W]	V_L [V]	I_L [A]	P_L [W]	η [%]	R_L [Ω]
30	0.535	15.863	20.088	0.569	11.443	72.136	50
30	0.372	11.098	20.296	0.389	7.909	71.270	68
30	0.282	8.418	20.556	0.291	5.992	71.182	100
30	0.193	5.809	20.880	0.196	4.095	70.499	150
30	0.133	4.035	20.826	0.133	2.781	68.919	220
30	0.094	2.842	21.012	0.092	1.942	68.358	470

Due to the converter input voltage being higher than the output voltage, it was observed that the input current (I_1) is greater than the output current (I_L), especially at high load values, and that the output current value reaches the input current value when the load value is reduced and then passes it. When the input and output current and voltage values are compared, it was observed that the converter efficiency is low at low power levels and the converter performance is high at high power levels.

Fig. 19 shows the variation of efficiency-output power for different output voltages (V_L) levels.

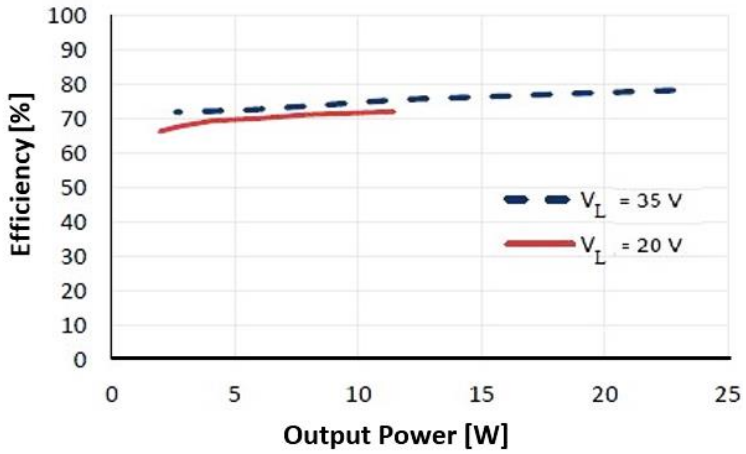

Fig. 19. Efficiency versus output power for different output voltage (V_L) levels.

Upon examining Fig. 19, it is apparent that the system efficiency decreases as the load voltage value decreases. Specifically, as the output voltage value decreases from 35 Volts to 20 Volts, the efficiency value also decreases. At the same power level, the current value in low voltage ($V_L = 20$ V) is higher than in high voltage ($V_L = 35$ V). Therefore, high current flow causes high switching power loss and results in lower efficiency, as shown in Fig. 19.

In an experimental setup, the single-phase off-grid transformerless H5 inverter system is controlled using PI and Fuzzy PI controllers. The performance of the controllers is evaluated based on the inverter output voltage and other performance criteria. Fig. 20 shows the inverter output and reference signals obtained from different controllers.

Variable values are used as reference voltage, as shown in Fig. 20. The system input is 50 Volts, and the reference voltages are determined as 10, 20, 30, and 15 Volts, respectively. It has been observed that the inverter output voltage follows the variable reference waveform. The obtained controller performance criteria are given in Table 11.

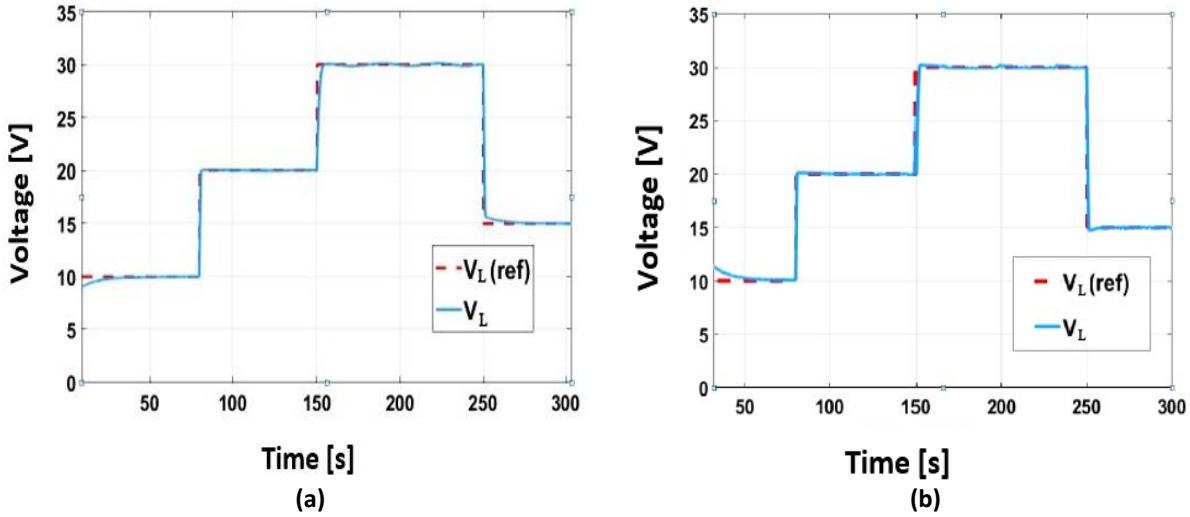

Fig. 20 (a) Output voltage and reference voltage (PI), (b) Output voltage and reference voltage (Fuzzy PI).

Table 11. Comparison of control methods.

Controller	ISE	IAE	ITAE
PI	1039	178.7	7697
Fuzzy PI	1013	170.9	5611

Table 11 shows that the Fuzzy PI controller outperforms the PI controller in terms of ISE, IAE, and ITAE performance criteria. In this study, a single-phase transformerless H5 inverter system is examined.

5. CONCLUSIONS

This study examined a single-phase transformerless H5 inverter system. Detailed grid-connected and off-grid system simulation studies were conducted using MATLAB/Simulink environment. The off-grid system simulation was compared with its experimental design, and the performance of the two was evaluated.

Based on the off-grid system simulation results, there is no phase difference between the current and voltage waveforms on the load. The THD value on the load is lower than the IEEE 1547 standard of 5%. Efficiency tests were conducted for different voltage values on the load, and a high output voltage value resulted in a 92% efficiency rating.

Furthermore, the system's output voltage has been regulated using both PI and Fuzzy PI controllers. The Fuzzy PI controller outperformed the PI controller in terms of ISE, IAE, and ITAE criteria. The grid-connected system's simulation results indicated no phase difference between the current and voltage waveforms injected into the grid. The grid THD value is below the 5% threshold specified in the IEEE 1547 standard.

The study also obtained values for active and reactive power flows to the grid. The active power injected into the grid varies according to the current and voltage values at the inverter output. It can be said that the reactive power is at a minimum level with this.

An experimental installation of the single-phase off-grid transformerless H5 inverter was completed. The system uses a TMS320DOCKF28335 digital processing unit to control and display the output voltage of the H5 inverter in real-time mode. Efficiency tests were conducted for different load voltage values, with an experimental study achieving 77.36% efficiency for the high output voltage specified in the simulation. It was observed that the efficiency increases as the voltage value of the load increases. The system output voltage was controlled using PI and Fuzzy PI controllers, which delivered better results in terms of ISE, IAE, and ITAE performance criteria.

Some limitations of the discussed techniques and topologies derived from the H-bridge include increased complexity and cost of the system. Additionally, the performance gains achieved by these methods may not be significant enough to justify the added complexity. Future research could investigate ways to simplify the implementation of these techniques and reduce their cost, as well as explore other modulation methods that may lead to even better results in terms of reactive power and efficiency.

Building on the previous discussion, it is also important to consider the practicality of implementing these techniques in real-world applications. For example, the availability and cost of components necessary for these systems may vary depending on location and industry. Additionally, the environmental impact of these systems should also be taken into account. Future research could explore the feasibility of implementing these techniques in different contexts and the potential environmental impacts of using these systems.

REFERENCES

[1] F. Dincer, E. Ozer, "Assessing the potential of a rooftop grid-connected photovoltaic system for Gaziantep islamic science and technology university/Turkey," *Jordan Journal of Electrical Engineering*, vol. 9, no. 2, pp. 149-165, 2023, doi: 10.5455/jjee.204-1670146602.

[2] O. Ahmed, M. Iqbal, "Design of a solar-powered water pumping system for irrigation in Sukkur, Pakistan," *Jordan Journal of Electrical Engineering*, vol. 9, no. 1, pp. 84-97, 2023, doi: 10.5455/jjee.204-1669679136.

[3] F. Faraji, A. Birjandi, S. Mousavi, J. Zhang, B. Wang, X. Guo, "An improved multilevel inverter for single-phase transformerless PV system," *IEEE Transactions on Energy Conversion*, vol. 36, no. 1, pp. 281–290, 2021, doi: 10.1109/TEC.2020.3006552.

[4] S. Dhara, A. Hota, S. Jain, V. Agarwal, "A transformerless 1-φ, 5-level half-bridge PV inverter configuration based on switched-capacitor technique," *IEEE Transactions on Industry Applications*, vol. 57, no. 2, pp. 1619–1628, 2021, doi: 10.1109/TIA.2021.3050975.

[5] H. Xiao, "Overview of transformerless photovoltaic grid-connected inverters," *IEEE Transaction on Power Electronics*, vol. 36, no. 1, pp. 533–548, 2021, doi: 10.1109/TPEL.2020.3003721.

[6] M. Kibria, A. Elsanabary, K. Tey, M. Mubin, S. Mekhilef, "A Comparative review on single phase transformerless inverter topologies for grid-connected photovoltaic systems," *Energies*, vol. 16, no. 3, p. 1363, 2023, doi: 10.3390/en16031363.

[7] V. Sonti, S. Jain, V. Agarwal, S. Bhattacharya, "Terminal voltage analysis for the transformerless PV inverter topologies in a single-phase system," *IET Renewable Power Generation*, vol. 13, no. 15, pp. 2723–2739, 2019, doi: 10.1049/IET-RPG.2019.0106.

[8] T. Duong, M. Nguyen, T. Tran, D. Vo, Y. Lim, J. Choi, "Topology review of three-phase two-level transformerless photovoltaic inverters for common-mode voltage reduction," *Energies*, vol. 15, no. 9, p. 3106, 2022, doi: 10.3390/en15093106

[9] M. Islam, M. Hasan, F. Badal, S. Das, S. Ghosh, "A blended improved H5 topology with ILQG controller to augment the performance of microgrid system for grid-connected operations," *IEEE Access*, vol. 8, pp. 69639–69660, 2020, doi: 10.1109/ACCESS.2020.2986213.

[10] F. Grigoletto, "Five-level transformerless inverter for single-phase solar photovoltaic applications," *IEEE Journal of Emerging and Selected Topics in Power Electronics*, vol. 8, no. 4, pp. 3411–3422, 2020, doi: 10.1109/JESTPE.2019.2891937.

[11] L. Jiang, Y. Chen, F. Dai, K. Liu, X. Chen, X. He, "A nine-switch inverter with reduced leakage current for PV grid-tied systems using model-free predictive current control," *Energy Reports*, vol. 9, no. 10, pp. 396-405, 2023, doi: 10.1016/j.egyr.2023.05.170.

[12] K. Kumar, A. Kirubakaran, N. Subrahmanyam, "Bidirectional clamping-based H5, HERIC, and H6 transformerless inverter topologies with reactive power capability," *IEEE Transactions on Industry Applications*, vol. 56, no. 5, pp. 5119–5128, 2020, doi: 10.1109/TIA.2020.2999552.

[13] Y. Syasegov, M. Farhangi, R. Barzegarkhoo, Y. Siwakoti, L. Li, D. Lu, R. Aguilera, J. Pou, "A 5-level HERIC active-clamped inverter with full reactive power capability for grid-connected applications," *IEEE Open Journal of the Industrial Electronics Society*, vol. 4, pp. 135-148, 2023, doi: 10.1109/OJIES.2023.3271637.

[14] Y. Syasegov, M. Farhangi, R. Barzegarkhoo, L. Li, D. Lu, R. Aguilera, Y. Siwakoti, "HERIC-clamped and PN-NPC inverters with five-level output voltage and reduced grid-interfaced filter size," *IEEE Open Journal of Power Electronics*, vol. 4, pp. 306-318, 2023, doi: 10.1109/OJPEL.2023.3265062.

[15] T. Kerekes, R. Teodorescu, P. Rodríguez, G. Vázquez, E. Aldabas, "A new high-efficiency single-phase transformerless PV inverter topology," *IEEE Transactions on Industrial Electronics*, vol. 58, no. 1, pp. 184–191, 2011, doi: 10.1109/TIE.2009.2024092.

[16] M. Khan, M. Forouzesh, Y. Siwakoti, L. Li, "Novel High Efficiency H-Bridge Transformerless Inverter for Grid-Connected Single-Phase Photovoltaic Systems," *IEEE Region Ten Symposium*, 2018, doi: 10.1109/TENCONSpring.2018.8692008.

[17] A. Datta, R. Sarker, "Improvements to the H5 inverter topology for transformer-less grid-photovoltaic interface applications," *IET Renewable Power Generation*, vol. 14, no. 11, pp. 1873–1882, 2020, doi: 10.1049/IET-RPG.2019.1199.

[18] W. Cha, K. Kim, Y. Cho, S. Lee, B. Kwon, "Evaluation and analysis of transformerless photovoltaic inverter topology for efficiency improvement and reduction of leakage current," *IET Power Electronics*, vol. 8, no. 2, pp. 255–267, 2015, doi: 10.1049/iet-pel.2014.0401.

[19] N. Vosoughi, S. Hosseini, M. Sabahi, "A New single-phase transformerless grid-connected inverter with boosting ability and common ground feature," *IEEE Transactions on Industrial Electronics*, vol. 67, no. 11, pp. 9313–9325, Nov. 2020, doi: 10.1109/TIE.2019.2952781.

[20] X. Guo, J. Zhou, R. He, X. Jia, C. Rojas, "Leakage current attenuation of a three-phase cascaded inverter for transformerless grid-connected PV systems," *IEEE Transactions on Industrial Electronics*, vol. 65, no. 1, pp. 676–686, 2018, doi: 10.1109/TIE.2017.2733427.

[21] F. Hadjbenali, F. Azzouz, "SPWM techniques for fifteen level flying capacitor inverter," *Jordan Journal of Electrical Engineering*, vol. 3, no. 3, pp. 181-192, 2017.

[22] L. Abdelhak, A. Benslimane, B. Jamal, M. El-Ouariachi, "Single-phase transformerless inverter topologies at different levels for a photovoltaic system, with proportional resonant controller," *International Journal of Electrical and Computer Engineering*, vol. 13, no. 2, pp. 1410-1422, 2023, doi: 10.11591/ijece.v13i2.pp1410-1422.

[23] *1547-2003 - IEEE Standard for Interconnecting Distributed Resources with Electric Power Systems*, 2003. https://ieeexplore.ieee.org/document/1225051.

[24] A. Yuksel, E. Ozkop, "Control of single phase grid connected transformerless PV inverter system," Pamukkale University Journal of Engineering Sciences, vol. 25, no. 2, pp. 143–150, 2019, doi: 10.5505/pajes.2018.93275.

[25] *TMDSDOCK28335 Development kit*, 2021, https://www.ti.com/tool/TMDSDOCK28335.